IOP PUBLISHING PLASMA PHYSICS AND CONTROLLED FUSION

Plasma Phys. Control. Fusion **49** (2007) B403–B410 doi:10.1088/0741-3335/49/12B/S37

GeV plasma accelerators driven in waveguides

S M Hooker[1], E Brunetti[2], E Esarey[3], J G Gallacher[2], C G R Geddes[3], A J Gonsalves[3], D A Jaroszynski[2], C Kamperidis[4], S Kneip[4], K Krushelnick[4], W P Leemans[3], S P D Mangles[4], C D Murphy[4,5], B Nagler[1], Z Najmudin[4], K Nakamura[3,6], P A Norreys[5], D Panasenko[3], T P Rowlands-Rees[1], C B Schroeder[3], C s Tóth[3] and R Trines[5]

[1] Department of Physics, University of Oxford, Clarendon Laboratory, Parks Road, Oxford, OX1 3PU, UK
[2] Department of Physics and Applied Physics, University of Strathclyde, John Anderson Building, 107 Rottenrow, Glasgow, UK
[3] Lawrence Berkeley National Laboratory, Building 71, 1 Cyclotron Road, Berkeley, CA 94720, USA
[4] Blackett Laboratory, Imperial College, Prince Consort Road, London, SW7 2BZ, UK
[5] Rutherford Appleton Laboratory, Chilton, Didcot, OX11 0QX, UK
[6] Nuclear Professional School, University of Tokyo, Tokyo, Japan

Received 6 July 2007
Published 19 November 2007
Online at stacks.iop.org/PPCF/49/B403

Abstract

During the last few years laser-driven plasma accelerators have been shown to generate quasi-monoenergetic electron beams with energies up to several hundred MeV. Extending the output energy of laser-driven plasma accelerators to the GeV range requires operation at plasma densities an order of magnitude lower, i.e. $10^{18}\,\mathrm{cm}^{-3}$, and increasing the distance over which acceleration is maintained from a few millimetres to a few tens of millimetres. One approach for achieving this is to guide the driving laser pulse in the plasma channel formed in a gas-filled capillary discharge waveguide. We present transverse interferometric measurements of the evolution of the plasma channel formed and compare these measurements with models of the capillary discharge. We describe in detail experiments performed at Lawrence Berkeley National Laboratory and at Rutherford Appleton Laboratory in which plasma accelerators were driven within this type of waveguide to generate quasi-monoenergetic electron beams with energies up to 1 GeV.

(Some figures in this article are in colour only in the electronic version)

1. Introduction

In the first demonstrations of the generation of quasi-monoenergetic electron beams by laser-driven plasma accelerators [1–3], electron energies of order 100 MeV were achieved by accelerating over distances of order 1 mm in plasmas with electron densities between 0.6×10^{19} and $2 \times 10^{19}\,\mathrm{cm}^{-3}$. Analytical expressions for both the laser wakefield and bubble regimes show that the maximum electron energy gain is proportional to n_e^{-1} if the other experimental

parameters are scaled so that the underlying assumptions remain valid [4]. Increasing the electron energy reached by a single stage to the GeV range is therefore expected to require operation at plasma densities of order $10^{18}\,\mathrm{cm}^{-3}$. However, since the dephasing distance L_d is proportional to $n_\mathrm{e}^{-3/2}$, decreasing the plasma density by an order of magnitude requires acceleration over tens of millimetres. This distance is significantly beyond the Rayleigh range of the driving laser beam, and hence GeV-class plasma accelerators require the laser pulse to be channelled by relativistic self-focusing and/or by a waveguide structure.

In this paper we describe one type of waveguide able to channel laser pulses with the peak intensities required for laser-driven acceleration: the gas-filled capillary discharge waveguide [5, 6]. We outline the operation of this type of plasma waveguide, present interferometric measurements of the evolution of the channel, and describe two experiments in which the waveguide was used to generate quasi-monoenergetic electron beams with energies up to 1 GeV.

2. The gas-filled capillary discharge waveguide

In a gas-filled capillary discharge waveguide a capillary formed in alumina or sapphire is filled with gas, usually hydrogen, via small holes located a few millimetres from each end of the capillary. A pulsed discharge current of several hundred amperes, and several hundred nanoseconds duration, is driven through the capillary via coaxial electrodes at each end of the capillary. The discharge is initiated by closing a high-voltage switch so as to connect a storage capacitor of 1–5 nF charged to a voltage of 10–30 kV.

Measurements [5, 7] and simulations [8, 9] show that a plasma channel is formed by the capillary discharge. In outline this occurs as follows. After electrical breakdown the hydrogen gas is dissociated and ionized to form an approximately uniform plasma. An axial minimum in the electron density is formed during the next few tens of nanoseconds as a result of thermal conduction to the capillary wall, which causes the plasma to be hotter on axis—and hence of lower density—than it is near the capillary wall. The temperature and density profiles formed are enhanced by a redistribution of electrical current towards the axis where the conductivity is higher. The plasma channel formed by these processes typically persists for many tens of nanoseconds, before axial flow of plasma out of the capillary and cooling of the plasma causes the axial density and curvature of the plasma channel to decrease.

3. Transverse interferometry of the plasma channel

We have measured the formation of the plasma channel by transverse interferometry [7]. To avoid refraction of the probe beams, capillaries of square cross-section formed by sandwiching thin sapphire spacer plates between optically flat sapphire blocks were employed.

Figure 1 shows the experimental arrangement. The capillary was placed in a Mach-Zehnder interferometer and probed transversely by $\approx$5 ns pulses at 532 and 1064 nm from a Nd : YAG laser. The virtual fringes formed in the plane of the capillary were imaged by a 75 mm focal length lens, the 532 and 1064 nm images being separated and directed to two CCD cameras by a mirror. A microscope objective was placed in front of each camera to magnify the fringe pattern, and transmission filters blocked the other probe beam. Fringe patterns were typically recorded at 10 ns intervals during the discharge pulse for initial hydrogen pressures between 10 and 150 mbar, and for peak discharge currents between 350 and 600 A.

The refractive index experienced by the probe beams arises almost entirely from the free electrons of the plasma and consequently the phase shift experienced by a probe beam of

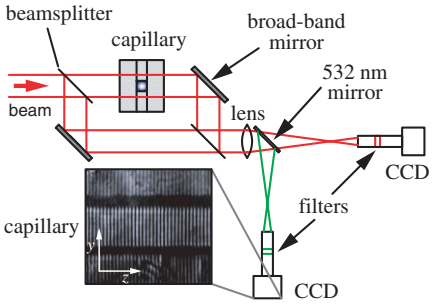

Figure 1. Transverse interferometry of the plasma channel. The inset shows the fringes formed by parts of the probe beam passing through, and either side of the channel.

wavelength λ is

$$\Phi_{\rm p}(y,z) = -r_{\rm e}\lambda \int_{-X/2}^{X/2} n_{\rm e}(x,y,z)\,{\rm d}x, \tag{1}$$

where X is the width of the capillary and the other co-ordinates are as illustrated in figure 1. However, the probe beams may also experience a further, time-dependent phase shift from changes in the optical thickness of the capillary wall arising from wall heating and expansion. Since the temperature-dependent terms of the refractive index of sapphire do not depend strongly on wavelength, it may be assumed that the phase shift arising from the wall, $\Phi_{\rm w}$, varies inversely with λ. By measuring the phase shifts $\Phi_{\rm m}^{\lambda_i}$ for two wavelengths λ_1 and λ_2, where $\lambda_1 = 2\lambda_1$, the phase shift arising from the plasma alone may be deduced. This model was confirmed by measuring the phase shift experienced by a third probe beam (not shown) which was reflected from the capillary wall [7].

The deduced phase shift arising from the plasma, $\Phi_{\rm p}(y,z)$, is proportional to the integral of the electron density along the x-axis. Reconstruction of the electron density profile was achieved by assuming that the electron density profile satisfies $n_{\rm e}(x,y,z) = f(x,z)f(y,z)$, where $f(x,z)$ may then be determined from the measured phase shift [7]. Tests of the reconstruction process on a simulated electron density profile showed that the axial electron density and matched spot of the recovered profile were within 10% of the original, simulated profile [7].

The matched spot size of a plasma channel is largely independent of the shape of the transverse electron density profile, and is given—to a very good approximation—by the smallest distance r from the axis for which the increase in the electron density above the axial value exceeds $(\pi r_{\rm e} r^2)^{-1}$ [10].

Figure 2(*a*) shows the deduced matched spot size (where the spot size is defined as the $1/e^2$ radius of the intensity profile) of the plasma channel formed in capillaries of side 465 μm as a function of the initial density of hydrogen molecules $n_{\rm H_2}^{\rm i}$. Also shown are the matched spot sizes calculated for *circular* cross-section capillaries of diameter X by the quasi-static model (QSM) of [8] and a non-local thermodynamic equilibrium (non-LTE) model [11]. It is seen that the measurements are in good agreement with both models. Experiments were also performed with capillaries of side 125 μm and 210 μm. Fitting all the data to a power law gives

$$W_{\rm M}\ (\mu{\rm m}) = 6.6\times 10^4 \left(\frac{X\ (\mu{\rm m})}{2}\right)^{0.651} (n_{\rm H_2}^{\rm i}\ ({\rm m}^{-3}))^{-0.1875}. \tag{2}$$

Figure 2(*b*) shows the measured axial electron densities together with the results of the QSM model and magnetohydrodynamic (MHD) calculations of [8], and the non-LTE simulations of [11]. It may be seen that the measured axial electron densities are in close

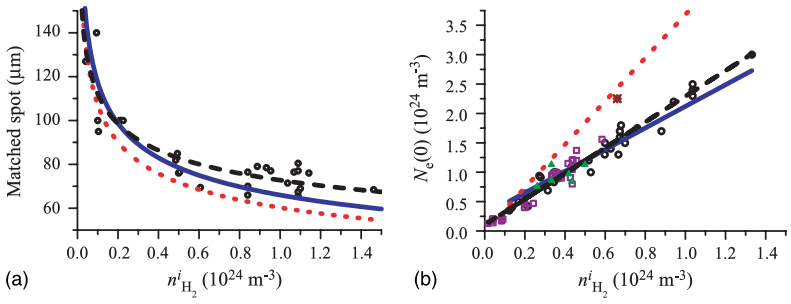

Figure 2. (*a*) Measured matched spot size as a function of $n^{\mathrm{i}}_{\mathrm{H}_2}$ for capillaries of side 465 μm. The dotted line shows W_{M} calculated by the QSM of [8], the solid line that by the non-LTE model of [11], and the dashed line is equation (2). (*b*) Deduced on-axis density as a function of $n^{\mathrm{i}}_{\mathrm{H}_2}$ for capillaries of side 125 μm (triangles), 210 μm (circles), 465 μm (squares). The on-axis density calculated by the QSM and the non-LTE simulations are shown by the dotted and solid lines, respectively. The dashed line is equation (3) and the star denotes the result of the MHD simulations of [11].

agreement with the predictions of the non-LTE simulation, but that the QSM model and the MHD calculations differ significantly from the measurements. The differences in the results of the models may be explained by the fact that in the QSM and MHD calculations the degree of ionization of the plasma near the capillary wall is unrealistically high [7].

A fit to all the measured data yields

$$n_{\mathrm{e}}(0)\ (\mathrm{m}^{-3}) = 0.87 n^{\mathrm{i}}_{\mathrm{H}_2}\ (\mathrm{m}^{-3}) + 0.11 \times 10^{24}. \tag{3}$$

4. Electron acceleration experiments

The gas-filled capillary discharge waveguide has recently been used in experiments performed at the Lawrence Berkeley National Laboratory (LBNL) [12, 13] and the Rutherford Appleton Laboratory (RAL) to significantly extend the distance over which electrons may be accelerated, and hence to increase the energies reached.

4.1. Experiments at LBNL

The experiments performed at LBNL utilized the high-power Ti : sapphire laser system of the LOASIS facility. As illustrated schematically in figure 3(*a*), laser pulses with a peak power of up to 40 TW were focused by an $f/25$ off-axis paraboloid to a waist of approximately 25 μm in the entrance plane of a gas-filled capillary discharge waveguide.

The capillaries used in this work were 33 mm long, with diameters of 190, 210 and 310 μm. The transverse intensity profile of the transmitted laser radiation was recorded by imaging the transmitted beam onto a CCD camera, the intensity of the beam having been reduced by reflecting from a pair of optically flat wedges. A pair of photodiodes monitored the energy of the laser pulse entering and exiting the waveguide.

The energy of electron beams generated within the waveguide was measured using a broadband electron spectrometer which employed a 1.2 T electromagnet to disperse the electrons onto four phosphor screens each imaged by a CCD camera. This arrangement allowed electrons with energies in the range 0.03–0.15 GeV and 0.175–1.1 GeV to be recorded in a single shot.

Electron beams were generated in all the capillary diameters investigated. The threshold intensity for injection and acceleration of electrons was investigated by adjusting the energy and duration of the driving laser pulse. It was found that the threshold intensity was lower

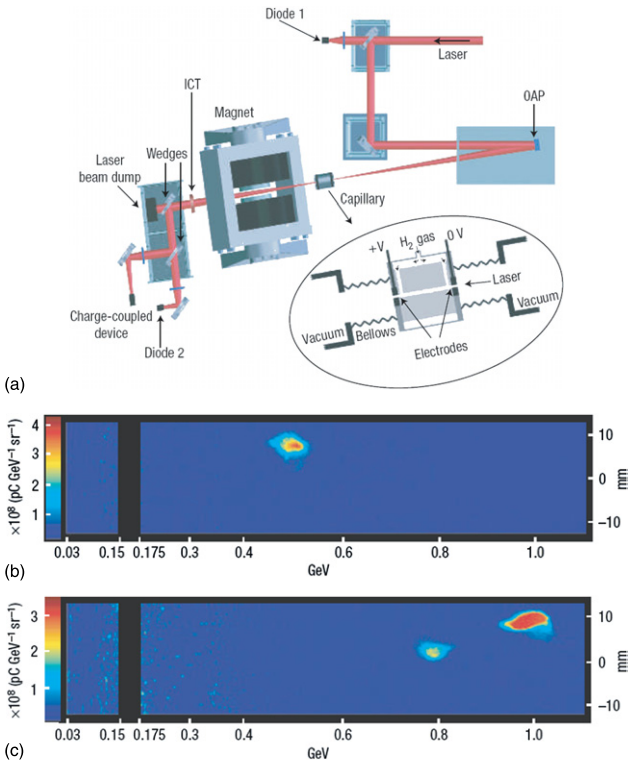

Figure 3. (*a*) Schematic diagram of the experimental arrangement employed in the Oxford-LBNL experiments. Quasi-monoenergetic electron beams generated at (*b*) $0.5^{+0.02}_{-0.015}$ GeV ($\Delta E = 5.6\%$ rms, $\Delta\theta = 2.0$ mrad, $Q \approx 50$ pC) obtained in a 225 μm capillary with 12 TW laser pulses and (*c*) $1.0^{+0.08}_{-0.05}$ GeV ($\Delta E = 2.5\%$ rms, $\Delta\theta = 1.6$ mrad, $Q \approx 30$ pC) obtained in a 310 μm capillary with 40 TW laser pulses.

for smaller diameter capillaries, and that charge Q, energy E, and energy spread ΔE of the generated beams depended critically on the delay t and on $n_e(0)$ [13].

Under certain conditions the electron beams generated were very stable. For example, figure 3(*b*) shows a single-shot electron spectrum obtained with a 225 μm diameter capillary and an input peak laser power of 12 TW. From equation (3) the axial electron density was $n_e(0) \approx 3.5 \times 10^{18}$ cm^{-3}. This 0.5 GeV beam was found to be highly reproducible: for delays t between 80 and 110 ns every laser shot with an energy within $\pm 5\%$ of that of figure 3(*b*), and focused to within 10 μm of the centre of the capillary, resulted in an electron beam with energies of 0.48 GeV $\pm$ 6% and a rms energy spread of less than 5%.

Higher energy electron beams were produced at higher laser powers in the 310 μm diameter capillary. Figure 3(*c*) shows an electron beam with an energy of 1 GeV produced by a laser pulse with a peak input power of 40 TW. The energy spread of this beam was measured to be less than 2.5% rms.

The 1 GeV beams were less stable than the 0.5 GeV beams of figure 3(*b*), possibly as a result of the greater mismatch between the input laser spot size and the matched spot of the plasma channel, weaker transverse variation of the plasma density in larger diameter capillaries, and greater sensitivity to small variations of the laser and plasma parameters at high laser powers.

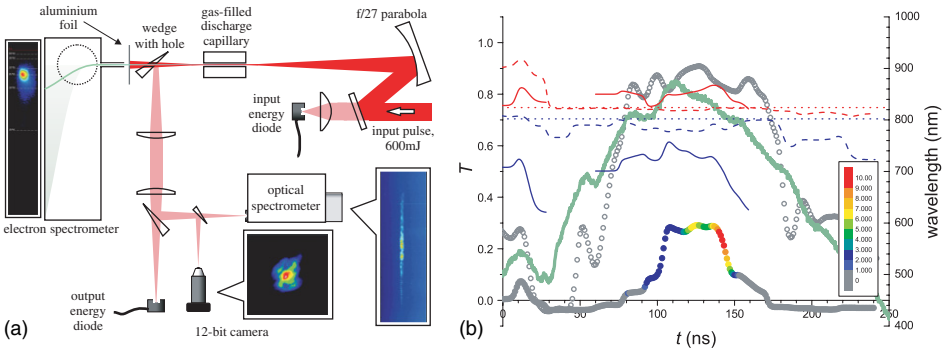

Figure 4. (*a*) Schematic diagram of the experimental arrangement employed in the RAL experiments. (*b*) Measured pulse energy transmission T, as a function of delay t for a 200 μm diameter capillary and $n_e(0) = 8.7 \times 10^{18}$ cm^{-3} for both long (open symbols) and short (closed symbols) laser pulses. The solid line gives the discharge current. On each transmission curve the charge of the generated electron beam is given in arbitrary units according to the colour scale. Also shown are the measured values of $\lambda_{R,B}$ of the spectrum of the transmitted long (dashed line) and short (solid line) laser pulses. The dotted lines give $\lambda_{R,B}$ for the input pulses. The curves plotted are running averages of the measured data.

4.2. Experiments at RAL

Recently we have undertaken further experiments using the Astra laser at RAL. The experimental arrangement was similar to the LBNL experiments, as illustrated in figure 4(*a*). A significant difference was that laser radiation leaving the waveguide was partially reflected by a wedge in which had been drilled along the propagation axis a hole of 4 mm diameter. The hole subtended an angle of 7 mrad at the exit of the waveguide, which was small enough not to degrade the measured image or spectrum of the transmitted laser radiation, but sufficiently large to transmit the generated electron beams. As a result it was possible to record simultaneously the energy spectrum of the electrons generated and the energy, spectrum, and transverse profile of the transmitted laser radiation.

The laser pulses, of energy 600 mJ, were focused to a waist of 30 μm in the entrance plane of the capillary. The laser was operated in two regimes. In the 'short pulse' regime the duration of the pulse was 45 fs, corresponding to a peak input intensity of 8×10^{17} W cm^{-2}, a peak power of 13 TW, and a normalized vector potential of $a_0 = 0.6$. In the 'long pulse' regime a compensating block of glass was removed from the laser path, prior to the compressor, which increased the pulse duration to approximately 150 fs and hence decreased the peak input intensity, peak power, and a_0 to 2.4×10^{17} W cm^{-2}, 4 TW, and 0.3, respectively.

Experiments were performed for 15 mm long capillaries of diameter 200 and 300 μm, for both long and short laser pulses, and for a range of initial hydrogen pressures. Energetic electron beams were only observed with short driving laser pulses, and only for 200 μm diameter capillaries.

Figure 4(*b*) shows the measured pulse energy transmission as a function of the delay t, for both long and short laser pulses, for a 200 μm capillary with $n_e(0) = 8.7 \times 10^{18}$ cm^{-3}. It is seen that for the long pulses the transmission forms a plateau with $T \approx 90\%$ lasting approximately 100 ns. The measured transverse fluence profiles of the transmitted pulses were found to be close to that of the input pulse for the range of delays approximately equal to that in which the *short* laser pulses exhibited a plateau of high transmission.

Figure 4(*b*) shows that for the short laser pulses the peak transmission was only approximately 30% and the duration of the plateau was reduced to approximately 40 ns. Even for delays corresponding to the plateau, the fluence profiles of the transmitted beams showed a more complex structure than those recorded with long pulses: for low initial pressures the transmitted beams comprised a small central spot and a larger, low-intensity beam with dimensions comparable to the capillary diameter. At higher pressures the transmitted beams were more severely distorted. For the 300 μm diameter capillaries, however, the peak transmission obtained with the short laser pulses was ≈90%.

In order to quantify the broadening of the spectra of the transmitted laser pulses, in figure 4(*b*) we plot the red (blue), λ_R (λ_B), limits of the measured spectra, corresponding to the wavelengths for which 15.9% of the spectrum lies at longer (shorter) wavelengths. It is seen that for the long laser pulses $\lambda_{R,B}$ remain close to those of the input spectrum during the plateau of high T. However, for short laser pulses λ_R and λ_B are shifted significantly from those of the input pulse throughout the interval for which the transmission is high. This extensive broadening reflects the much stronger interaction with the plasma of the channel experienced by the short laser pulse.

Electron beams were generated with the short laser pulse and 200 μm diameter capillaries for a range of initial pressures. For initial pressures corresponding to $n_e(0) \lesssim 3.5 \times 10^{18}\,\mathrm{cm}^{-3}$, only low-energy, broad-bandwidth electron beams were generated. Quasi-monoenergetic beams were generated for $6.5 \times 10^{18}\,\mathrm{cm}^{-3} \lesssim n_e(0) \lesssim 1.3 \times 10^{19}\,\mathrm{cm}^{-3}$. The energy of the quasi-monoenergetic peak was observed to increase from approximately 150 MeV for $n_e(0) \approx 6.5 \times 10^{18}\,\mathrm{cm}^{-3}$ to a maximum of 200 MeV for $n_e(0) \approx 8.7 \times 10^{18}\,\mathrm{cm}^{-3}$, and decreased to approximately 150 MeV for $n_e(0) \approx 1.3 \times 10^{19}\,\mathrm{cm}^{-3}$.

Figure 4(*b*) also shows the beam charge recorded by the electron spectrometer as a function of the delay t. From this it is clear that electron beams were generated only for a short range of delays within the interval for which the laser pulses were transmitted with high transmission.

We may make several observations. Channelling of the short laser pulses, and generation of electron beams, was very sensitive to the capillary diameter: for 300 μm diameter capillaries the peak transmission for short laser pulses was generally higher than in the 200 μm diameter capillaries, and no electrons were generated; for 200 μm diameter capillaries a significant decrease in the peak transmission compared to that obtained with long laser pulses coincided with generation of energetic electron beams. For the 200 μm diameter capillaries the shorter duration of the plateau in T observed for the short laser pulses indicates that the channelling of the short laser pulses depends much more critically on the properties of the plasma channel than is the case for the long pulses. This increased sensitivity is expected since the amplitude of the laser wakefield will be greater, and relativistic self-focusing will be more significant, for the short pulses. For example: for $n_e(0) \approx 8.7 \times 10^{18}\,\mathrm{cm}^{-3}$, $P_{\mathrm{laser}}/P_{\mathrm{crit}} \approx 4$ for the short pulses compared with $P_{\mathrm{laser}}/P_{\mathrm{crit}} \approx 1$ for the long pulses.

It is interesting to note that for the 200 μm diameter capillaries significant spectral broadening of the transmitted pulses—indicating wakefield formation [14]—were found to occur throughout the range of delays for which high transmission was observed, but electron beams were only observed for a much narrower range of delays. This observation suggests that strong wakefields were generated for a relatively wide range of delays, but that electron injection depends sensitively on the properties of the plasma channel.

5. Conclusions

The gas-filled capillary discharge waveguide is a versatile method for creating plasma waveguides able to guide high-intensity laser pulses over several tens of millimetres. Models

of the formation of the plasma channel are in good agreement with transverse interferometric measurements, and scaling laws have been determined for the two key parameters, the axial electron density and the matched spot size.

We have used this waveguide to extend by an order of magnitude the distance over which electrons can be accelerated in a laser-driven accelerator, and in so doing have generated quasi-monoenergetic electron beams with energies as high as 1 GeV. These experiments are the first time that a laser-driven accelerator has reached energies comparable to those used in many conventional radio-frequency-based facilities.

The experiments performed at LBNL and RAL suggest that for a given input laser intensity the probability of injection is greater for smaller diameter capillaries. This behaviour may arise from the smaller matched spot size of the plasma channel for smaller diameter capillaries (equation (2)) which will affect both the propagation of the driving laser pulse, and could also increase the magnitude of the transverse wakefield. Further, the RAL experiments demonstrate—at least for relatively low laser energies—that injection of electrons depends critically on the delay t, although guiding of long, lower-intensity pulses is relatively insensitive to this parameter. These results suggest that electron injection may be sensitive to subtle properties of the plasma channel—issues which we are investigating through numerical modelling and longitudinally resolved interferometric measurements of the evolution of the plasma channel. We conclude by noting that this sensitivity offers an opportunity for control—as witnessed by the generation of very stable 0.5 GeV electron beams—and expect that tailoring the properties of the plasma channel will enable further control to be achieved.

References

[1] Mangles S P D *et al* 2004 Monoenergetic beams of relativistic electrons from intense laser–plasma interactions *Nature* **431** 535–8

[2] Geddes C G R, Tóth C, van Tilborg J, Esarey E, Schroeder C B, Bruhwiler D, Nieter C, Cary J and Leemans W P 2004 High-quality electron beams from a laser wakefield accelerator using plasma-channel guiding *Nature* **431** 538–41

[3] Faure J, Glinec Y, Pukhov A, Kiselev S, Gordienko S, Lefebvre E, Rousseau J P, Burgy F and Malka V 2004 A laser–plasma accelerator producing monoenergetic electron beams *Nature* **431** 541–4

[4] Leemans W, Esarey E, Geddes C, Schroeder C and Tóth C 2006 Laser guiding for GeV laser–plasma accelerators *Phil. Trans. R. Soc. A—Math. Phys. Eng. Sci.* **364** 585–600

[5] Spence D J and Hooker S M 2001 Investigation of a hydrogen plasma waveguide *Phys. Rev.* E **6302** 015401

[6] Butler A, Spence D J and Hooker S M 2002 Guiding of high-intensity laser pulses with a hydrogen-filled capillary discharge waveguide *Phys. Rev. Lett.* **89** 185003

[7] Gonsalves A J, Rowlands-Rees T P, Broks B H P, van der Mullen J J A M and Hooker S M 2007 Transverse interferometry of a hydrogen-filled capillary discharge waveguide *Phys. Rev. Lett.* **98** 025002

[8] Bobrova N A, Esaulov A A, Sakai J I, Sasorov P V, Spence D J, Butler A, Hooker S M and Bulanov S V 2002 Simulations of a hydrogen-filled capillary discharge waveguide *Phys. Rev.* E **65** 016407

[9] Broks B H P, Garloff K and van der Mullen J J A M 2005 Nonlocal-thermal-equilibrium model of a pulsed capillary discharge waveguide *Phys. Rev.* E **71** 016401

[10] Durfee C G, Lynch J and Milchberg H M 1994 Mode properties of a plasma wave-guide for intense laser-pulses *Opt. Lett.* **19** 1937–9

[11] Broks B H P, van Dijk W and van der Mullen J J A M 2006 Parameter study of a pulsed capillary discharge waveguide *J. Phys. D: Appl. Phys.* **39** 2377–83

[12] Leemans W P, Nagler B, Gonsalves A J, Tóth C S, Nakamura K, Geddes C G R, Esarey E, Schroeder C B and Hooker S M 2006 GeV electron beams from a centimetre-scale accelerator *Nature Phys.* **2** 696–9

[13] Nakamura K, Nagler B, Tóth C S, Geddes C G R, Schroeder C B, Esarey E, Leemans W P, Gonsalves A J and Hooker S M 2006 GeV electron beams from a centimetre-scale channel guided laser wakefield accelerator *Phys. Plasmas* **14** 056708

[14] Murphy C D *et al* 2006 Evidence of photon acceleration by laser wake fields *Phys. Plasmas* **13** 033108